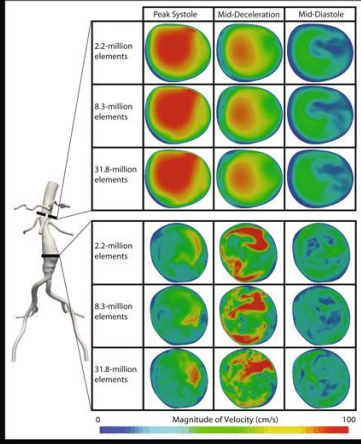



ISSN 0090-6964, Volume 38, Number 4


ISSN: 0090-6964 • Volume: 38 • Number: 4 • April 2010

Annals of
Biomedical Engineering



A Journal of the Biomedical Engineering Society

 **BMES**
BIOMEDICAL ENGINEERING SOCIETY™
Advancing Human Health and Well-Being™

 Springer

Available
online
www.springerlink.com

**This article was published in the above mentioned Springer issue.
The material, including all portions thereof, is protected by copyright;
all rights are held exclusively by Springer Science + Business Media.
The material is for personal use only;
commercial use is not permitted.
Unauthorized reproduction, transfer and/or use
may be a violation of criminal as well as civil law.**

Effects of Scleral Stiffness Properties on Optic Nerve Head Biomechanics

ARMIN EILAGHI,^{1,2} JOHN G. FLANAGAN,^{3,4} CRAIG A. SIMMONS,^{1,2} and C. ROSS ETHIER^{1,2,3,5}

¹Department of Mechanical and Industrial Engineering, University of Toronto, Toronto, Canada; ²Institute of Biomaterials and Biomedical Engineering, University of Toronto, Toronto, Canada; ³Department of Ophthalmology and Vision Sciences, University of Toronto, Toronto, Canada; ⁴Optometry School, University of Waterloo, Waterloo, Canada; and ⁵Department of Bioengineering, Imperial College London, Exhibition Road, London SW7 2AZ, UK

(Received 25 August 2009; accepted 16 December 2009; published online 29 December 2009)

Associate Editor Bahman Anvari oversaw the review of this article.

Abstract—The biomechanical environment within the optic nerve head, important in glaucoma, depends strongly on scleral biomechanical properties. Here we use a range of measured nonlinear scleral stress–strain relationships in a finite element (FE) model of the eye to compute the biomechanical environment in the optic nerve head at three levels of intraocular pressure (IOP). Three stress–strain relationships consistent with the 5th, 50th and 95th percentiles of measured human scleral stiffness were selected from a pool of 30 scleral samples taken from 10 eyes and implemented in a generic FE model of the eye using a hyperelastic five-parameter Mooney-Rivlin material model. Computed strains within optic nerve head tissues depended strongly on scleral properties, with most of this difference occurring between the compliant and median scenarios. Also, the magnitudes of strains were found to be substantial even at normal IOP (up to 5.25% in the lamina cribrosa at 15 mmHg), being larger than previously reported values even at normal levels of IOP. We conclude that scleras that are “weak”, but still within the physiologic range, will result in appreciably increased optic nerve head strains and could represent a risk factor for glaucomatous optic neuropathy. Estimations of the deformation at the optic nerve head region, particularly at elevated IOP, should take into account the nonlinear nature of scleral stiffness.

Keywords—Finite element modeling, Sclera, Optic nerve head, Glaucoma.

INTRODUCTION

Glaucoma is a group of potentially blinding ocular diseases characterized by gradual and progressive damage to the optic nerve, and is usually associated with elevated intraocular pressure (IOP).¹ The cause of vision loss in glaucoma is damage to the axons of the

retinal ganglion cells (the retinal nerve fibers) at the optic nerve head (ONH, see Fig. 1 and the related caption for anatomic description). Because IOP is generally acknowledged to be the major risk factor for the initiation and development of glaucoma,³ and because lowering of IOP is currently the only efficacious treatment for this disease,¹⁴ IOP-related biomechanical factors are hypothesized to play a key role in the glaucomatous damage process. There is, therefore, considerable interest in studying the effects of IOP on ONH biomechanics.^{4,23}

The biomechanics of the optic nerve head are complex due to the presence of various mechanically different tissues interacting with each other,⁵ as well as the considerable inter-individual variability in the geometry of this region.¹³ ONH tissues undergo multiple modes of strain²⁸ in response to changes in IOP. Bellezza *et al.*² studied IOP-related stresses within the ONH using finite element (FE) modeling and found scleral canal size and shape and scleral thickness to be the most important geometrical factors affecting ONH stresses in human eyes. Sigal *et al.* established FE models of the human ONH using generic²⁶ and individual-specific^{24,27} geometries. Sensitivity analysis using their models showed that the stiffness of the sclera had the largest effect on ONH strains.^{24,27} These studies show that ONH biomechanics are strongly influenced by scleral stiffness and thickness, highlighting the importance of implementing realistic models of scleral properties for studying ONH biomechanics.

The above studies assumed that the sclera was linearly elastic. However, there is evidence that the stress–strain behavior of the sclera is nonlinear.^{7,31,32} Also, scleral stiffness at low IOP (<10 mmHg) can be substantially lower than stiffnesses previously used in finite element models^{7,11} and may vary amongst

Address correspondence to C. Ross Ethier, Department of Bioengineering, Imperial College London, Exhibition Road, London SW7 2AZ, UK. Electronic mail: r.ethier@imperial.ac.uk

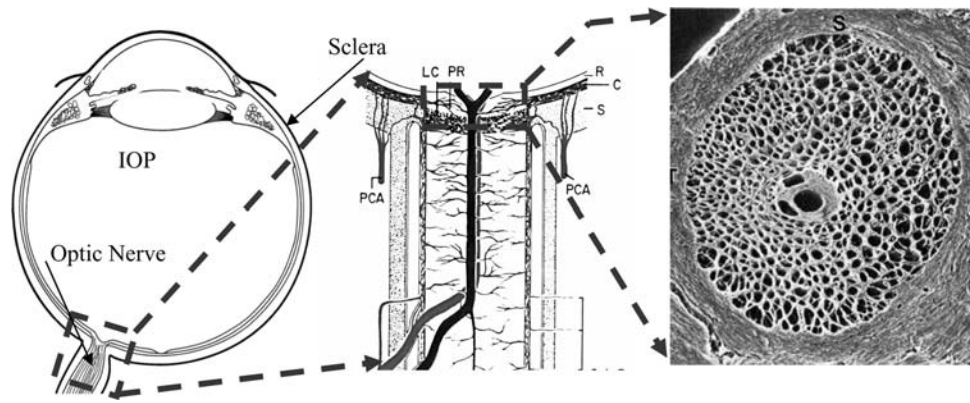


FIGURE 1. Left panel: cross-sectional overview through a human eye. The boxed region is the optic nerve head area, and is shown magnified in the middle panel¹²: Overview of the major anatomical features of the optic nerve head. Symbols: LC, Lamina Cribrosa; PCA, Posterior ciliary arteries; C, choroid; R, retina; S, sclera. Right panel: en face view of the lamina cribrosa, showing connective tissue elements only.¹⁷ The pores, through which the nerve fibers pass, can be clearly seen.⁸

individuals. In the current research we used measured stress–strain relationships for human scleral samples, representative of stiff, median and compliant scleras, and implemented these nonlinear material properties in a generic finite element model of the human eye to compute the biomechanical environment in the ONH at three levels of IOP.

METHODS

The results of biaxial extensional testing on scleral samples taken from ten ostensibly normal eyes from five human donors (age 55.4 ± 3.5 years, mean \pm standard deviation) were used as input for this research. The stress–strain data, based on samples taken from the sclera approximately 3 mm from the center of the optic nerve, showed nonlinear and near-isotropic behavior.⁷ As described in detail elsewhere,⁷ the data were fit to the 4-parameter Fung model

$$W = c(e^Q - 1), \quad Q = c_1 E_{11}^2 + c_2 E_{22}^2 + 2c_3 E_{11} E_{22} \quad (1)$$

$$S_{ij} = \frac{\partial W}{\partial E_{ij}} \quad (2)$$

where W , c 's, E_{ij} and S_{ij} are the Fung strain energy function, material parameters, Green strains and Kirchoff stresses, respectively.

When c_3 is small (which it was for our data), and when the strain is small, the products c^*c_1 and c^*c_2 can be interpreted as measures of stiffness of a sample in directions 1 and 2, respectively; in our tests the “1” and “2” directions were polar (azimuthal) and circumferential, respectively. The samples were ordered according to the value of $c^*(c_1 + c_2)/2$, as a single measure of stiffness, and 5th, 50th and 95th percentile values of the resulting distribution were calculated.

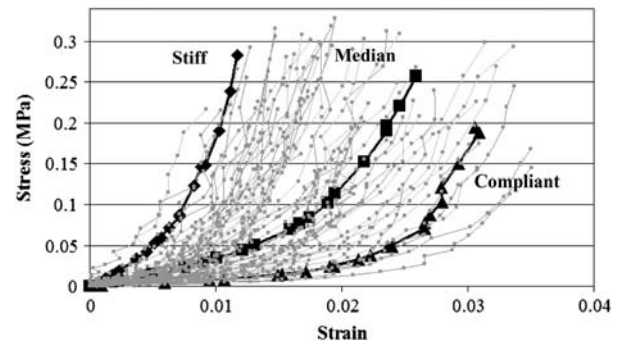


FIGURE 2. Variation in biaxial stiffness of sclera. The raw data is shown as gray dots in the background (30 samples). Samples were sorted according to their measures of stiffness,⁷ and three samples that were closest to the 5th, 50th and 95th percentile values of the stiffness distribution were selected as the compliant, median and stiff scenarios, respectively, as described in the text.

Samples which were closest to those values were selected as “compliant”, “median” and “stiff” samples for the finite element modeling work described below (Fig. 2).

A previously reported axisymmetric generic human eye geometry^{24,27} was used for all finite element modeling (Fig. 3). The ONH is represented in more detail than the rest of the eye in this model, and includes five tissues: the prelaminar neural tissue (PNT), which includes all neural tissue anterior to the lamina cribrosa within 15° of the axis of symmetry; the lamina cribrosa (LC); the retrolaminar neural tissue (RNT); the pia mater (PM); and the peripapillary sclera (PPS), defined to be scleral tissue within 15° of the axis of symmetry. Further than 15° away from the axis of symmetry, the corneo-scleral shell (SS) was assumed to be a spherical shell of uniform thickness. Retinal shell tissue (RS) extended anteriorly to 105° from the center of the ONH.

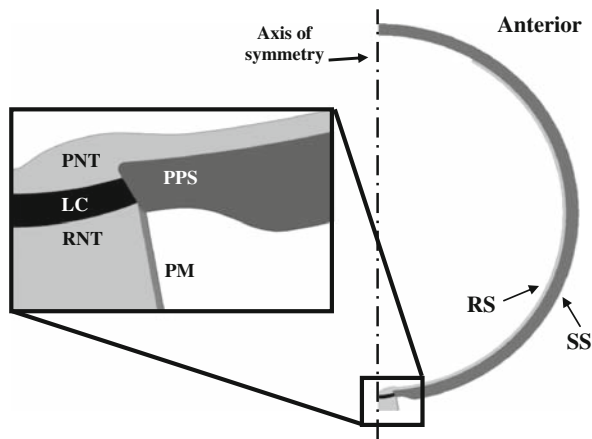


FIGURE 3. Axisymmetric model geometry used for finite element computations in this study, based on Sigal *et al.*²⁶ The scleral shell (SS) is shown in dark gray, with a magnified view of the ONH region shown as an inset. The scleral tissue was divided into two parts: the peripapillary sclera (PPS, including the sclera from the wall of the scleral canal) to 15° from the axis of symmetry, and the scleral shell (SS) which includes the rest of the corneo-scleral shell. The prelaminar neural tissue (PNT) also includes the neural tissue anterior to the LC and retina anterior to the peripapillary sclera. (Symbols: SS, scleral shell; RS, retinal shell; PPS, peripapillary sclera; PNT, prelaminar neural tissue; LC, lamina cribrosa; RNT, retrolaminar neural tissue; PM, pia mater.)

The measured stress-strain behaviors of the sclera (Fig. 2) were implemented in the commercial finite element modeling package ANSYS 11.0 (ANSYS Inc., Canonsburg, PA) as a 5-parameter Mooney-Rivlin model. The other tissues in the model were assumed to be isotropic and linearly elastic (Table 1). This approach was selected based on several factors: sclera is the stiffest tissue in the ONH region so that the deformation of the ONH tissues depends strongly on scleral deformation⁹; and the paucity of mechanical testing data for other ONH tissues.²⁶

Uniform intraocular pressures of 15, 25, and 50 mmHg were applied to all interior surfaces of the eye. Nodes on the axis of symmetry at the anterior pole

of the eye were fixed in all directions, while nodes on the symmetry axis at the posterior pole of eye (the center of the ONH region) were constrained to deform along this axis of symmetry. Eight node elements (PLANE82 in ANSYS) were used throughout. A mesh refinement analysis was performed to ensure that the models were sufficiently resolved. The final models had 6,644 elements and 20,911 nodes.

The outcomes of our computations are presented in terms of principal strains, since there is evidence to suggest that cellular behavior is controlled by strain (deformation) rather than directly by stress.²¹ For each tissue region and for each principal strain, the 50th and 95th percentiles of nodal strain values were calculated as a measure of median and peak strains, respectively. The reason for using the 95th percentile value is to eliminate the influence of possible outliers and to thus provide more realistic values of the peak principal strains. It is important to note that 50th and 95th percentiles of nodal principal strain values should not be interpreted as the average and peak deformation state in the tissue region because the spatial direction for the principal strains will in general vary from point to point. However, these metrics provide an indication of the cellular-level mechanical insult that a cell may undergo in each tissue region.

RESULTS

Our results show that as IOP is increased, peripapillary sclera (PPS) and lamina cribrosa (LC) displace posteriorly while the scleral canal expands (Fig. 4a), consistent with previous finding.⁴ The overall effect is to create appreciable levels of strain and a complex strain field in the LC and PPS (Fig. 4b).

Regardless of scleral properties, the magnitudes of the third principal strain were higher than the first principal strain in all optic nerve head tissues, suggesting that these tissues undergo more compression

TABLE 1. Summary of the mechanical properties of the ONH tissues used in our models.

ONH tissue	Material model	Type	Material parameters				
			C ₁₀	C ₀₁	C ₁₁	C ₂₀	C ₀₂
Sclera	Hyperelastic and Incompressible	S ^a	3.26E+2	-3.25E+2	-3.41E+7	1.74E+7	1.67E+7
		M ^b	5.45E+1	-5.41E+1	-1.05E+6	5.45E+5	5.07E+5
		C ^c	6.78	-6.73	-1.13E+5	5.85E+4	5.43E+4
Lamina cribrosa	Linearly elastic and incompressible	Elastic Modulus = 0.3 MPa, Poisson's Ratio = 0.49 ^{25,26}					
Retina	Linearly elastic and incompressible	Elastic Modulus = 0.03 MPa, Poisson's Ratio = 0.49 ^{25,26}					
Pia mater	Linearly elastic and incompressible	Elastic Modulus = 3 MPa, Poisson's Ratio = 0.49 ^{25,26}					

^aStiff scenario.

^bMedian scenario.

^cCompliant scenario.

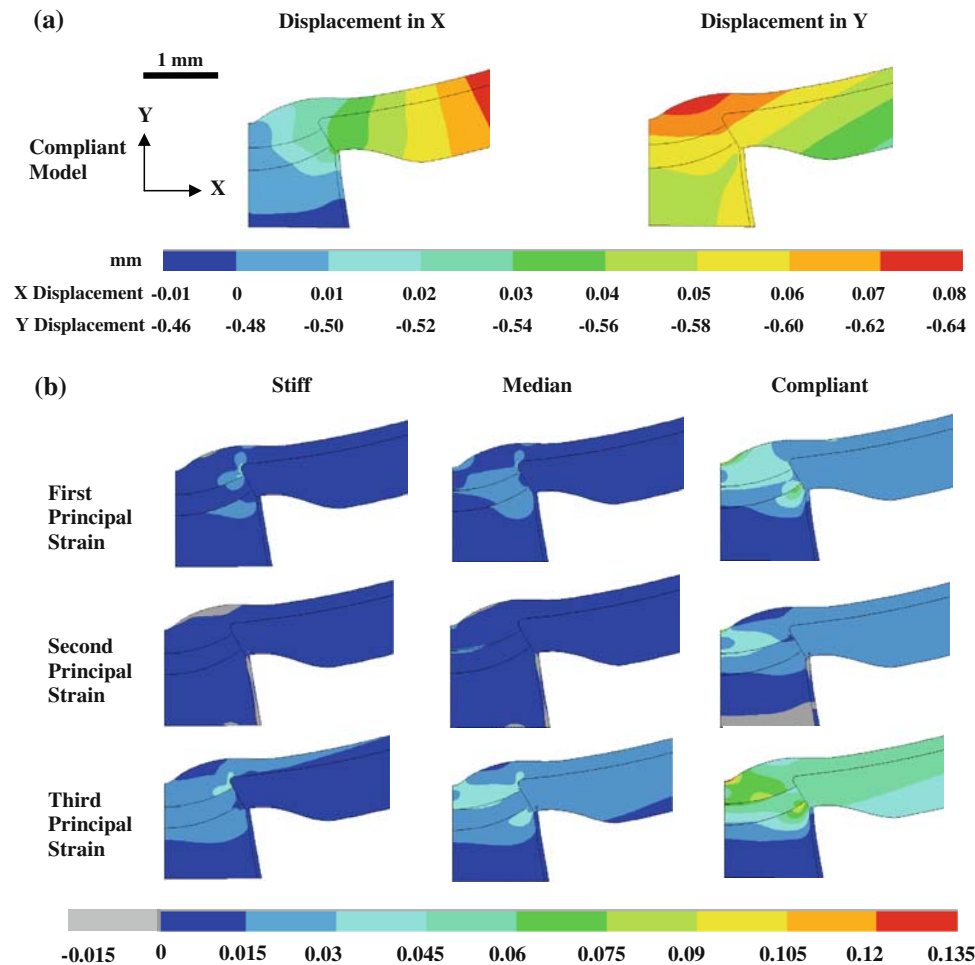


FIGURE 4. (a) Computed displacement in X and Y directions for the compliant scleral stiffness scenario, measured with respect to the zero pressure configuration. As IOP increased, optic nerve head tissues (including peripapillary sclera and lamina cribrosa) displaced posteriorly (i.e. in the negative Y direction) while the scleral canal expanded (X direction). Note the difference between contour levels of panels. (b) Computed principal strain distributions in ONH and peripapillary tissues at an IOP of 25 mmHg, for three different sets of scleral mechanical properties: stiff sclera, median sclera and compliant sclera (see Fig. 3). See text for further description of different models. The absolute value of the third principal strain is shown to facilitate comparison.

than extension (Fig. 4), as previously observed.²⁸ The peak magnitudes of the first and third principal strains were greatest in the neural tissues (PNT and RNT) and were slightly larger than values computed in the LC (Fig. 5). However, the LC showed the highest level of median strain and greatest homogeneity in the strain amongst the ONH tissues. The patterns of the principal strains and displacement distribution in ONH tissues (Fig. 4) suggest that as scleral properties changed, both compressive (third) and extensional (first) principal strains substantially increased in two regions: 1) The optic cup, which in our classification (Fig. 3) is part of the prelaminar neural tissue (PNT) region, and 2) the peripheral part of the retrolaminar neural (RNT) tissue where this tissue attaches to the peripapillary sclera and LC. The above comments hold at all three IOP levels.

Even at normal IOPs, the magnitudes of strains were found to be substantial. For example, at an IOP of 15 mmHg with the compliant sclera scenario, the third principal strain magnitudes were 5.3, 5.8 and 6.2% in the LC, prelaminar and retrolaminar neural tissues, respectively. At an IOP of 50 mmHg, these values increased to 8.8, 10.4 and 9.6%, respectively.

The magnitudes of principal strains differed significantly (Fig. 5) between models with different scleral material properties. As expected, the differences between models were greatest in the scleral tissues (SS and PPS regions in Fig. 3); however, there were also large differences in both compressive and extensive modes of strain in other optic nerve head tissues, namely the prelaminar neural tissue, LC and retrolaminar neural tissue. For example, at an IOP of 25 mmHg the peak value of the first principal strain in

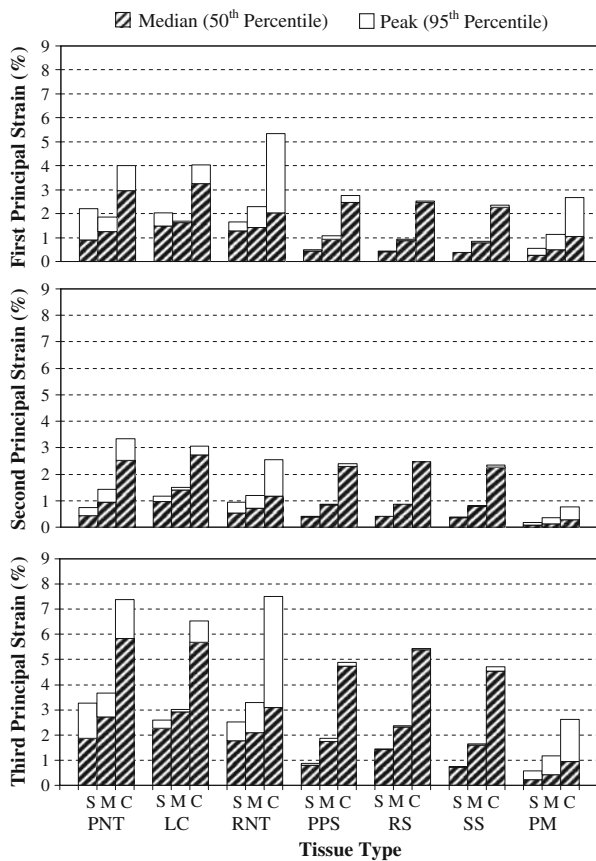


FIGURE 5. The effects of scleral mechanical properties on median (50th percentile) and peak (95th percentile) principal strains within tissues of the optic nerve head, retinal and scleral shells at 25 mmHg. The absolute value of the third principal strain is shown to facilitate comparison. S, M and C refer to models with stiff, median and compliant scleral mechanical properties, respectively. See legend of Fig. 2 for further nomenclature.

the peripapillary sclera (PPS) differed by 457% between the stiff and compliant scenarios, with corresponding strain differences of 82% in the PNT, 98% in the LC and 221% in the RNT. The differences in magnitudes of the third principal strain between models with stiff and compliant sclera were even higher. For example, when comparing the models with compliant and stiff scleras, the peak magnitude of the third principal strain differed by 126% in the PNT, 151% in the LC and 197% in the RNT (Fig. 5). Generally speaking, the median scenario resulted in strains that were reasonably close to the stiff scenario, i.e., the majority of the change in going from a compliant to a stiff sclera occurred in the change from compliant to median scenarios.

Increasing IOP had different effects in models with different scleral stiffness (Fig. 6). As one would expect, the stiffer sclera resulted in lower deformation of all ONH tissues. However, in models with stiffer scleral material properties, the magnitudes of the principal

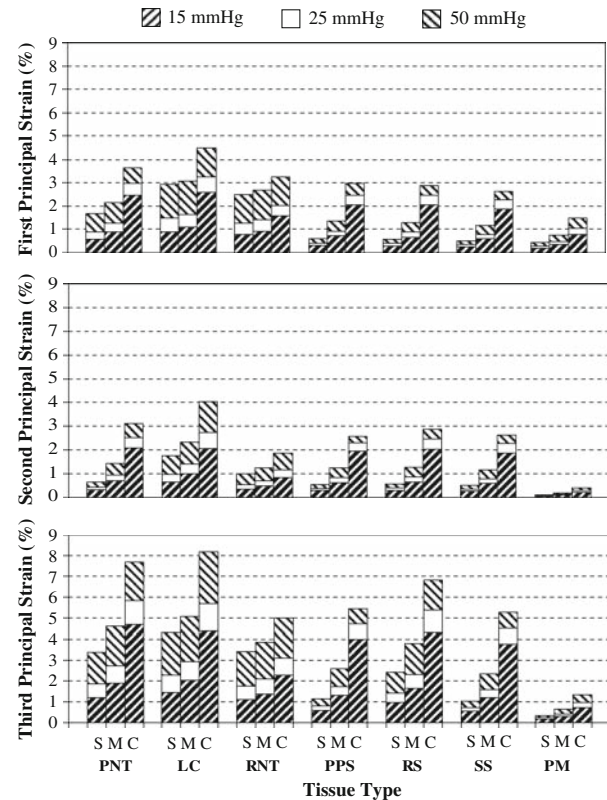


FIGURE 6. The effects of changing IOP on median (50th percentile) principal strains within tissues of the optic nerve head, retinal and scleral shells. S, M and C refer to models with stiff, median and compliant scleral mechanical properties, respectively. The absolute value of the third principal strain is shown to facilitate comparison. See legend of Fig. 3 for further nomenclature.

strains increased at a higher rate as IOP was increased than was the case in more compliant models. For example, as a result of doubling the IOP from 25 to 50 mmHg the median first principal strain increased by 70% in models with stiff sclera but by only 25% in models with compliant sclera (averaged amongst all 7 tissues). Interestingly, the maximum proportional increase in strains due to increasing IOP occurred in the LC. For example, when IOP increased from 25 to 50 mmHg, the peak values of the first principal strain in the LC increased by 114% in the model with a stiff sclera but by only 24% in the model with a compliant sclera. Similarly, the peak magnitudes of the third principal strain in the LC increased by 98% in the model with a stiff sclera and by only 35% in the model with a compliant sclera.

DISCUSSION

These data suggest that a compliant (but nonetheless apparently physiologic) sclera leads to substantial

strains in the tissues of the ONH; for example, the third principal strain was as high as 10% at an elevated IOP of 50 mmHg in the compliant sclera scenario. There is evidence from *in vitro* experiments that strains of 5–8% induce a wide range of biological effects in neural cells.^{6,10,16,18} Considering that the model with median scleral stiffness properties showed an ONH biomechanical environment closer to the stiff scenario than to the compliant scenario (Figs. 4–6), we conclude that IOP-induced deformation dramatically increases in eyes that belong to the lower range of physiologic scleral stiffness (“weak” scleras). Such eyes may be at increased risk of glaucomatous visual field loss at a given level of IOP. Thus, these results continue to support the idea that scleral mechanical properties strongly affect optic nerve head biomechanics, including the biomechanical environment within the lamina cribrosa.

The scleral stress–strain relationships used in this study were obtained from a pool of eyes that were ostensibly free of disease and were representative of the broader population as far as we are aware. It is of interest to consider individuals suffering from disorders that weaken connective tissues (e.g., Marfan’s syndrome, osteogenesis imperfecta, Ehlers-Danlos syndrome), who might be expected to show behavior close to, or even more compliant than, our compliant scenario. Such eyes would be expected to experience a high level of deformation at the optic nerve head region and could be at increased risk of glaucomatous optic neuropathy. Marfan’s patients show ocular abnormalities including increased axial length¹⁹ and enlarged globes that may indirectly contribute to the risk of glaucomatous damage,¹⁵ but have not been directly linked to retinal ganglion cell death. It appears that little is known about the natural history of glaucoma in these (relatively rare) connective tissue disorders, and it would be of interest to further investigate this issue.

On the other hand, stiffening the scleral matrix, through for example promoting collagen cross-linking,^{20,22,31} will decrease scleral deformation especially at physiologically meaningful (i.e. lower) loads. This is expected to diminish the IOP-induced strain in the ONH region. Our results predict that this could have some neuroprotective benefit, at least in patients with “weak” scleras.

Our models suggested that as IOP increased, peripapillary sclera (PPS) and lamina cribrosa (LC) displaced posteriorly (Fig. 4b) and simultaneously the scleral canal expanded (displaced in *X* direction) consistent with previous findings.⁴ In practice, scleral canal expansion may oppose and limit the posterior displacement of LC however substantial levels of strain will be induced in LC and PPS accordingly.

Increasing IOP from 15 to 25 mmHg and further to 50 mmHg highlighted the important effect of the nonlinearity in scleral stiffness. As a result of this nonlinearity, the rate of ONH deformation decreased as IOP increased. Interestingly, the model with a compliant sclera showed the lowest rate of increase in principal strains as a result of increasing IOP from 15 to 50 mmHg. The nonlinear stress-strain behavior in scleral stiffness was apparent at relatively low levels of IOP, consistent with Girard *et al.*¹¹ and Eilaghi⁷ This highlights the importance of taking into account the nonlinear pattern of scleral stiffness for computing the biomechanical environment of the optic nerve head region, particularly at elevated IOPs.

The models used in this study have limitations and involve assumptions which should be considered when interpreting the results derived from them. These include: (1) The finite element models were based on a simplified and generic geometry. (2) The material properties of the tissues other than sclera were assumed to be linearly elastic. (3) Our models computed the mean-field strain values in a tissue, without accounting for local tissue architecture. In the case of the lamina cribrosa the tissue micro-architecture can lead to local amplification of mean-field strains, increasing the actual strain experienced by the cells by up to an order of magnitude.³ (4) The sclera was modeled as a nonlinear isotropic material based on previous measurements⁷ on scleral samples taken from a subset of entire sclera away from the optic nerve and muscle attachments. However, some level of anisotropy may exist in the unmeasured regions, e.g., due to preferred fiber orientation.^{29,30} Further work should characterize a greater proportion of the human sclera and use this more complete data set in finite element models.

ACKNOWLEDGMENTS

Funding was provided through the Canadian Institute of Health Research (JGF, CRE) and the Canada Research Chairs Program (CRE).

REFERENCES

- ¹Allingham, R. R., and M. B. Shields. Shields’ Textbook of Glaucoma. Philadelphia: Lippincott Williams & Wilkins, 2005.
- ²Bellezza, A. J., R. T. Hart, and C. F. Burgoyne. The optic nerve head as a biomechanical structure: initial finite element modeling. *Invest. Ophthalmol. Vis. Sci.* 10:2991–3000, 2000.
- ³Burgoyne, C. F., J. C. Downs, A. J. Bellezza, J. K. Suh, and R. T. Hart. The optic nerve head as a biomechanical

- structure: a new paradigm for understanding the role of IOP-related stress and strain in the pathophysiology of glaucomatous optic nerve head damage. *Prog. Retin. Eye Res.* 1:39–73, 2005.
- ⁴Downs, J. C., M. D. Roberts, and C. F. Burgoyne. Mechanical environment of the optic nerve head in glaucoma. *Optom. Vis. Sci.* 6:425–435, 2008.
- ⁵Drance, S. M. *Optic Nerve in Glaucoma*. New York: Kugler Publications, 1995.
- ⁶Edwards, M. E., S. S. Wang, and T. A. Good. Role of viscoelastic properties of differentiated SH-SY5Y human neuroblastoma cells in cyclic shear stress injury. *Biotechnol. Prog.* 4:760–767, 2001.
- ⁷Eilaghi, A. Effects of scleral stiffness on biomechanics of the optic nerve head in glaucoma. PhD Dissertation, University of Toronto, 2009, pp. 57–72.
- ⁸Eilaghi, A., J. G. Flanagan, G. W. Brodland, and C. R. Ethier. Strain uniformity in biaxial specimens is highly sensitive to attachment details. *J. Biomech. Eng.* 131(9):091003, 2009.
- ⁹Ethier, C. R. Scleral biomechanics and glaucoma—a connection? *Can. J. Ophthalmol.* 1:9–14, 2006.
- ¹⁰Ethier, C. R., and C. A. Simmons. *Introductory Biomechanics: From Cells to Organisms*. Cambridge: Cambridge University Press, 2007.
- ¹¹Girard, M. J. A., J. C. Downs, C. F. Burgoyne, and J. F. Suh. Experimental surface strain mapping of porcine peripapillary sclera due to elevations of intraocular pressure. *J. Biomech. Eng.* 130(4):041017, 2008.
- ¹²Hayreh, S. S. *Anterior Ischemic Optic Neuropathy*. Berlin: Springer-Verlag, 1975.
- ¹³Jonas, J. B., P. Martus, F. K. Horn, A. Jünemann, M. Korth, and W. M. Budde. Predictive factors of the optic nerve head for development or progression of glaucomatous visual field loss. *Invest. Ophthalmol. Vis. Sci.* 8:2613–2618, 2004.
- ¹⁴Kass, M. A., D. K. Heuer, E. J. Higginbotham, C. A. Johnson, J. L. Keltner, J. Philip Miller, R. K. Parrish, II, M. Roy Wilson, and M. O. Gordon. The Ocular Hypertension Treatment Study: a randomized trial determines that topical ocular hypotensive medication delays or prevents the onset of primary open-angle glaucoma. *Arch. Ophthalmol.* 6:701–713, 2002.
- ¹⁵Krupin, T., R. Ritch, and M. B. Shields. *The Glaucomas*. St. Louis: Mosby, 1996.
- ¹⁶Margulies, S. S., and L. E. Thibault. A proposed tolerance criterion for diffuse axonal injury in man. *J. Biomech.* 8:917–923, 1992.
- ¹⁷Minckler, D. S. Histology of optic nerve damage in ocular hypertension and early glaucoma. *Surv. Ophthalmol. (Suppl.)* 33:401–402, 1989.
- ¹⁸Morrison III, B., H. L. Cater, C. C. Wang, F. C. Thomas, C. T. Hung, G. A. Ateshian, and L. E. Sundstrom. A tissue level tolerance criterion for living brain developed with an in vitro model of traumatic mechanical loading. *Stapp Car Crash J.* 47:93–105, 2003.
- ¹⁹Nelson, L. B., and I. H. Maumenee. Ectopia lentis. *Surv. Ophthalmol.* 3:143–160, 1982.
- ²⁰Pinsky, P. M., D. Van Der Heide, and D. Chernyak. Computational modeling of mechanical anisotropy in the cornea and sclera. *J. Cataract Refract. Surg.* 1:136–145, 2005.
- ²¹Saez, A., A. Buguin, P. Silberzan, and B. Ladoux. Is the mechanical activity of epithelial cells controlled by deformations or forces? *Biophys. J.* 6:L52–L54, 2005.
- ²²Schultz, D. S., J. C. Lotz, S. M. Lee, M. L. Trinidad, and J. M. Stewart. Structural factors that mediate scleral stiffness. *Invest. Ophthalmol. Vis. Sci.* 10:4232–4236, 2008.
- ²³Sigal, I. A., and C. R. Ethier. Biomechanics of the optic nerve head. *Exp. Eye Res.* 4:799–807, 2009.
- ²⁴Sigal, I. A., J. G. Flanagan, and C. R. Ethier. Factors influencing optic nerve head biomechanics. *Invest. Ophthalmol. Vis. Sci.* 11:4189–4199, 2005.
- ²⁵Sigal, I. A., J. G. Flanagan, and C. R. Ethier. Interactions between factors influencing optic nerve head biomechanics. In: 2007 ASME Summer Bioengineering Conference, SBC 2007, Keystone, CO, 2007.
- ²⁶Sigal, I. A., J. G. Flanagan, I. Tertinegg, and C. R. Ethier. Finite element modeling of optic nerve head biomechanics. *Invest. Ophthalmol. Vis. Sci.* 12:4378–4387, 2004.
- ²⁷Sigal, I. A., J. G. Flanagan, I. Tertinegg, and C. R. Ethier. Reconstruction of human optic nerve heads for finite element modeling. *Technol. Health Care* 4:313–329, 2005.
- ²⁸Sigal, I. A., J. G. Flanagan, I. Tertinegg, and C. R. Ethier. Predicted extension, compression and shearing of optic nerve head tissues. *Exp. Eye Res.* 3:312–322, 2007.
- ²⁹Thale, A., and B. Tillmann. The collagen architecture of the sclera—SEM and immunohistochemical studies. *Ann. Anat.* 3:215–220, 1993.
- ³⁰Thale, A., B. Tillmann, and R. Rochels. SEM studies of the collagen architecture of the human lamina cribrosa: normal and pathological findings. *Ophthalmologica* 3:142–147, 1996.
- ³¹Wollensak, G., and E. Spoerl. Collagen crosslinking of human and porcine sclera. *J. Cataract Refract. Surg.* 3:689–695, 2004.
- ³²Woo, S. L., A. S. Kobayashi, W. A. Schlegel, and C. Lawrence. Nonlinear material properties of intact cornea and sclera. *Exp. Eye Res.* 1:29–39, 1972.